

Fluid-Phase Coexistence for the Oxidation of CO₂ Expanded Cyclohexane: Experiment, Molecular Simulation, and COSMO-SAC

T. Merker

Laboratory of Engineering Thermodynamics, University of Kaiserslautern, 67663 Kaiserslautern, Germany

C.-M. Hsieh

Dept. of Chemical Engineering, National Taiwan University, 10617 Taipei, Taiwan

S.-T. Lin

Dept. of Chemical Engineering, National Taiwan University, 10617 Taipei, Taiwan

H. Hasse

Laboratory of Engineering Thermodynamics, University of Kaiserslautern, 67663 Kaiserslautern, Germany

J. Vrabec

Thermodynamics and Energy Technology, University of Paderborn, 33098 Paderborn, Germany

DOI 10.1002/aic.13986

Published online January 25, 2013 in Wiley Online Library (wileyonlinelibrary.com)

The gas solubility of pure oxygen and of pure carbon dioxide as well as of their gaseous mixture are measured in the ternary liquid mixture cyclohexane + cyclohexanone + cyclohexanol at 313.6 K with a high-pressure view-cell technique using the synthetic method. The new experimental data are used to assess the capability of molecular simulation and conductor-like screening model (COSMO)-SAC to predict multicomponent fluid-phase coexistence behavior. These methods are also compared systematically on the basis of experimental binary fluid-phase coexistence data. In that comparison also the Peng–Robinson (PR) equation of state is included as a reference. Molecular simulation and COSMO-SAC yield good results and are found to be far superior to the PR equation of state both in predictive and in adjusted mode. © 2013 American Institute of Chemical Engineers AIChE J, 59: 2236–2250, 2013

Keywords: oxygen, carbon dioxide, cyclohexane, cyclohexanone, cyclohexanol, experiment, gas solubility, Henry's law constant, molecular simulation, conductor-like screening model, COSMO-SAC, Peng–Robinson equation of state

Introduction

The oxidation of cyclohexane to cyclohexanol and cyclohexanone is an important industrial reaction and a key step in the nylon production chain. Usually, the reaction is carried out by contacting liquid cyclohexane with air at 398–438 K and 0.8–1.5 MPa. To avoid oxidative side reactions, this process step must be carried out at a low conversion rate of about 10% so that an acceptable selectivity of about 85% toward cyclohexanone and cyclohexanol is achieved.¹

Alternative routes are being studied for this process step. One option is the use of novel octahedral molecular sieves for the heterogeneously catalyzed selective oxidation of cyclohexane.² Another option is the use of supercritical carbon dioxide to expand the reactive liquid, which enhances the mobility of both the reactants and the products, to obtain a higher conversion rate and a better yield.³ Carbon dioxide

expanded reaction media may have additional benefits, such as better heat and mass transfer. A detailed review on the advantages of using supercritical carbon dioxide in such processes was recently published by Seki and Baiker.⁴

For a rational planning of catalytic experiments and the design of carbon dioxide expanded oxidation processes, especially because they take place at elevated pressures, phase equilibrium data are needed. For ternary and higher mixtures, the available experimental data base is very narrow. Thus, gas solubility and Henry's law constant data were measured for carbon dioxide in liquid mixtures of cyclohexane + cyclohexanone in Ref. 5. These results were compared to molecular simulation data in Ref. 6. Moreover, experimental and molecular simulation results for the Henry's law constant of pure oxygen and of pure carbon dioxide in cyclohexanol were reported in Ref. 7. Although some important subsystems were studied with respect to fluid-phase coexistence in our preceding work,^{5–7} the present study covers all five major components involved in the oxidation of carbon dioxide expanded cyclohexane in a systematic manner.

To the best of our knowledge, for systems containing more than three of the five relevant components, only a single source is publicly available: Esmelindro et al.⁸ published

Additional Supporting Information may be found in the online version of this article.

Correspondence concerning this article should be addressed to J. Vrabec at jadran.vrabec@upb.de.

experimental gas solubility data for carbon dioxide in the equimolar liquid mixture cyclohexane + cyclohexanone + cyclohexanol at temperatures between 293 and 343 K. For oxygen or for the mixture oxygen + carbon dioxide, no such data are available in the literature. In the present work, new experimental results for the gas solubility of oxygen and of carbon dioxide as well as of their gaseous mixture in the ternary liquid mixture cyclohexane + cyclohexanone + cyclohexanol are reported that cover a broad range of states.

Molecular modeling and simulation with classical force fields is a suitable method for the prediction of thermophysical properties of pure fluids and mixtures.^{9–13} It is based on mathematical representations of the intermolecular interactions and has good predictive capabilities. This approach adequately covers structure, energetics, and dynamics on the microscopic scale that govern the fluid behavior on the macroscopic scale. On the basis of given molecular force field models, the full variety of thermophysical properties, such as structural, thermal, caloric, transport, or phase equilibrium data, can be determined by molecular simulation. Due to the advent of computing power as a commodity, molecular simulations are now often much faster and much cheaper than experiments in the laboratory. In addition to yielding information on the properties of bulk fluids, molecular simulation allows for detailed insights into a fluid's structure and kinetics, for example, within nanostructured catalysts, which are difficult to obtain by experiment and are inaccessible by continuum models. However, a prerequisite for such studies are validated molecular models.

For quickly generating phase equilibrium data, for example, in process simulations, aggregated numerical expressions such as equations of state (EOS) or excess Gibbs free energy g^E models are needed. Conductor-like screening model (COSMO)-type g^E models^{14–17} and the Peng–Robinson (PR) EOS¹⁸ are widely used to model the phase behavior of multicomponent mixtures, for example, for process simulations.¹⁹ It is of interest to study the performance of these approaches to describe and predict fluid-phase coexistence in the present case. Such a study was carried out here for all 10 binary subsystems and also for most multicomponent systems up to the pentenary mixture oxygen + carbon dioxide + cyclohexane + cyclohexanone + cyclohexanol. Results from molecular simulation, the COSMO, and the PR EOS¹⁸ with and without one adjusted binary parameter were compared to experimental data.

In recent years, the COSMO for real solvents (COSMO-RS)^{14,20,21} as well as its variants COSMO-SAC (SAC denotes the segment activity coefficient model),^{15,22,23} COSMO-RS(OI) (OI denotes the COSMO-RS from Gmehling and Gmehling at the University of Oldenburg),¹⁶ and COSMO-vac¹⁷ have gained significant attention. Compared to more traditional predictive approaches such as UNI-FAC (UNIQUAC Functional-group Activity Coefficients),²⁴ COSMO-type models do not depend on tabulated model parameters because they solely require the results of quantum mechanical solvation calculations as an input to provide phase equilibrium predictions. They, thus, never suffer from missing parameter values and are applicable to a wider range of chemical species. This is particularly important for the industrial environment, where often new or little known compounds are of interest.

The COSMO approaches determine the activity coefficients of incompressible liquid mixtures on the basis of molecular surface interactions that are assumed to be dominated by local electrostatic interactions. This directly leads to g^E data that have to be supplied to an EOS by means of a

mixing rule if compressible fluids are of interest. In this work, the COSMO-SAC model^{15,22,23} was selected. It uses results from quantum mechanical software package DMol3 implemented in Materials Studio.²⁵ A database of the QM calculation results maintained by the Liu research group^{26,27} is also freely available to the public.²⁸ The COSMO approach, in combination with an EOS, is suitable to calculate Henry's law constant.^{29,30} The Peng–Robinson–Stryjek–Vera (PRSV) EOS³¹ in combination with the first-order modified Huron–Vidal mixing rule³² was used here.

The PR EOS in its classical form¹⁸ with the van der Waals mixing rule was considered in this work too because it is a widely used workhorse in the chemical industry. It only requires three input numbers for each component, that is, the critical values for temperature and pressure as well as one vapor pressure that is reformulated into the acentric factor. The PR EOS¹⁸ was considered here to define a cubic EOS baseline.

The performance of these three theoretical approaches was assessed here on the basis of experimental data in four steps. First, the capability of molecular simulation, COSMO-SAC, and the PR EOS to predict and describe mixture VLE data solely based on information of the pure components was studied for all 10 binary subsystems that can be formed from the five components mentioned above (predictive mode). Second, for each system, one data point was selected to adjust the binary parameter of each of the three models and the results were compared (adjusted mode). Third, predictions by molecular simulation and COSMO-SAC (both adjusted to binary data) were compared for six ternary mixtures. Fourth, the present experimental data for two quaternary mixtures and the pentenary mixture were compared to molecular simulation and COSMO-SAC (both adjusted to binary data).

Experiment

A synthetic method was applied for the present experimental study of gas solubility, and the employed apparatus was the same as in previous works of our laboratory.^{33–37} In the experiment, the pressure was determined that is required to dissolve a precisely known amount of a gas in a precisely known amount of a solvent. The central element of the apparatus is a thermostatted cylindrical high-pressure view cell (volume about 30 cm³) with two sapphire windows on each end.

During an experiment, the cell was initially evacuated. Then, for pure gases, the gas was charged into the cell from a gas cylinder. Its mass was determined volumetrically, from the known volume of the cell and from readings for temperature and pressure, by applying an EOS for the pure gas. In case of gaseous mixtures, oxygen was charged first and its mass was determined volumetrically as described above. Carbon dioxide was subsequently charged into the cell from a gas cylinder. The mass of carbon dioxide was determined gravimetrically by weighing the gas cylinder before and after the charging process with a high-precision balance. Solvent mixtures were also prepared gravimetrically. Next, the solvent mixture was added into the cell by means of a high-pressure spindle press until the gas was completely dissolved in the liquid.

After equilibration, small amounts of the solvent were withdrawn in a stepwise fashion until the first very small stable gas bubbles appeared. The pressure p at which the degassing starts is the solubility pressure. The mass of the solvent was calculated from the volume displacement in the calibrated spindle press and the solvent density. The

Table 1. Gas Solubility of Oxygen (1) and of Carbon Dioxide (2) in two Ternary Liquid Mixtures (A and B) that are Composed of Cyclohexane (3) + Cyclohexanone (4) + Cyclohexanol (5) at 313.6 K from Experiment

Mixture A			Mixture B		
x_1 (mol mol ⁻¹)	x_2 (mol mol ⁻¹)	p^σ (MPa)	x_1 (mol mol ⁻¹)	x_2 (mol mol ⁻¹)	p^σ (MPa)
0.016 (1)	–	2.09 (2)	0.025 (1)	–	2.28 (2)
0.025 (1)	–	3.34 (2)	0.035 (1)	–	3.17 (2)
0.035 (1)	–	4.66 (2)	0.046 (1)	–	4.25 (2)
0.043 (1)	–	5.88 (2)	0.066 (1)	–	6.17 (2)
0.064 (1)	–	8.86 (2)	0.073 (1)	–	6.92 (2)
–	0.093 (2)	1.14 (2)	–	0.072 (1)	0.97 (2)
–	0.141 (3)	1.68 (2)	–	0.095 (2)	1.24 (2)
–	0.174 (3)	2.04 (2)	–	0.109 (2)	1.43 (2)
–	0.187 (3)	2.20 (2)	–	0.140 (2)	1.76 (2)
–	0.230 (4)	2.68 (2)	–	0.159 (2)	1.98 (2)
–	0.245 (4)	2.80 (2)	–	0.249 (4)	2.99 (2)
–	0.316 (5)	3.57 (2)	–	0.322 (5)	3.71 (2)
0.024 (1)	0.079 (3)	4.08 (2)	0.083 (1)	–	8.07 (2)
0.024 (1)	0.101 (4)	4.19 (2)	0.025 (1)	0.068 (3)	3.05 (2)
0.023 (1)	0.132 (5)	4.45 (2)	0.024 (1)	0.117 (5)	3.57 (2)
0.023 (1)	0.160 (7)	4.64 (2)	0.024 (1)	0.164 (7)	4.02 (2)
0.022 (1)	0.194 (8)	4.94 (2)	0.023 (1)	0.168 (7)	4.06 (2)
0.022 (1)	0.25 (1)	5.36 (2)	0.045 (1)	0.045 (1)	4.59 (2)
0.044 (1)	0.093 (2)	6.73 (2)	0.044 (1)	0.093 (2)	5.06 (2)
0.043 (1)	0.096 (2)	6.58 (2)	0.044 (1)	0.120 (3)	5.39 (2)
0.043 (1)	0.112 (3)	6.81 (2)	0.043 (1)	0.160 (4)	5.68 (2)
0.042 (1)	0.124 (3)	6.82 (2)	0.042 (1)	0.168 (4)	5.74 (2)
0.041 (1)	0.163 (4)	7.08 (2)			

Mixture A: $x'_3 = 0.325$ mol mol⁻¹, $x'_4 = 0.35$ mol mol⁻¹, $x'_5 = 0.325$ mol mol⁻¹. Mixture B: $x'_3 = 0.764$ mol mol⁻¹, $x'_4 = 0.119$ mol mol⁻¹, $x'_5 = 0.117$ mol mol⁻¹, where x'_i are the gas free liquid mole fractions. The number in parentheses indicates the experimental uncertainty in the last digit.

solvent density was separately measured with a vibrating tube densimeter (model DMA 4500 M, Anton Paar).

Two calibrated platinum resistance thermometers in the thermostating jacket of the view cell were used to determine the temperature. The solubility pressure was measured with a pressure transducer (WIKA, full scale 10 MPa) in connection with a mercury barometer (Lambrecht). All pressure transducers were calibrated against a high-precision pressure balance (Desgranges & Huot).

The maximum uncertainty of the present solubility pressure measurements is due to the intrinsic uncertainty of the pressure transducers (0.1% of the transducer's full scale, i.e., 0.01 MPa here) and an additional contribution of about 0.01 MPa from a small temperature drift inside the isolated high-pressure tubes that connect the view cell with the pressure transducer. The uncertainty of the temperature measurement is ± 0.1 K.

Oxygen and carbon dioxide (both with a volume fraction 99.995%) were purchased from Messer Griesheim, Germany. Cyclohexane, cyclohexanone, and cyclohexanol (all with a purity $\geq 99.0\%$) were purchased from Sigma-Aldrich, Germany and degassed in our laboratory under vacuum.

The mole fraction based Henry's law constant $H_{i,j}(T, \mathbf{x})$ of pure oxygen and of pure carbon dioxide (solute i) in the solvent mixture j with the composition \mathbf{x} expressed in terms of the mole fraction vector $\mathbf{x} = (x_1, x_2, \dots)$ at the vapor pressure of the solvent mixture $p_j(T, \mathbf{x})$ was determined from the present experimental data using an extrapolation procedure

$$H_{i,j}(T, \mathbf{x}) = \lim_{p \rightarrow p_j} \left[\frac{f_i(T, p, \mathbf{y})}{x_i} \right], \quad (1)$$

where

$$f_i(T, p, \mathbf{y}) = py_i \varphi_i(T, p, \mathbf{y}). \quad (2)$$

The fugacity of the gaseous solute i is f_i and its fugacity coefficient is φ_i . x_i and y_i are the mole fractions of the solute i in the liquid and the vapor phase, respectively. $\mathbf{y} =$

(y_1, y_2, \dots) is the mole fraction vector that characterizes the vapor phase composition. Note that $H_{i,j}$ was determined only for systems that either contain oxygen or carbon dioxide, but not for systems that contain both gases.

The vapor pressure of the solvent mixture p_j was determined by molecular simulation because of the lack of experimental data. The employed molecular models were validated on the basis of other experimental data from the literature including our own previous work (see below). As the vapor pressure of the solvent mixture is low, it was assumed for the calculation of φ_i that the vapor consists only of the solute gas, that is, $y_i = 1$. The vapor-phase fugacity coefficient φ_i of the pure gases was calculated with the EOS by Schmidt and Wagner³⁸ for oxygen and the EOS by Span and Wagner³⁹ for carbon dioxide, respectively.

Numbers for f_i/x_i determined from the isothermal experimental data of pure oxygen and of pure carbon dioxide in two mixtures are shown in Supporting Information. The extrapolation Eq. (1) was done by linear regression. The resulting numerical data for the solubility pressure are given in Table 1 and for the Henry's law constant in Table 2, which also contains information on the estimated accuracy of the experimental data.

Molecular Simulation

All pure substance molecular force field models were taken from preceding work of our group. Oxygen⁴⁰ and carbon dioxide⁴¹ were described with two and three Lennard-Jones (LJ) sites, respectively, and one point quadrupole. Cyclohexane⁶ was modeled with six LJ sites and cyclohexanone⁶ was described with seven LJ sites and one point dipole. The cyclohexanol model⁴² consists of seven LJ sites and three point charges that cover electrostatics and hydrogen bonding. All employed molecular models were assumed to be rigid.

Table 2. Henry's Law Constant of Oxygen (1) and of Carbon Dioxide (2) in two Ternary Liquid Mixtures (A and B) that are Composed of Cyclohexane (3) + Cyclohexanone (4) + Cyclohexanol (5) at 313.6 K from Experiment and Molecular Simulation

Mixture <i>j</i>	Oxygen		Carbon Dioxide	
	H_{1j}^{exp} (MPa)	H_{1j}^{sim} (MPa)	H_{2j}^{exp} (MPa)	H_{2j}^{sim} (MPa)
A	132 (8)	122.6 (3)	12.5 (3)	12.4 (4)
B	91 (4)	86.8 (2)	13.8 (3)	12.7 (3)

Mixture A: $x'_3 = 0.325 \text{ mol mol}^{-1}$, $x'_4 = 0.35 \text{ mol mol}^{-1}$, $x'_5 = 0.325 \text{ mol mol}^{-1}$. Mixture B: $x'_3 = 0.764 \text{ mol mol}^{-1}$, $x'_4 = 0.119 \text{ mol mol}^{-1}$, $x'_5 = 0.117 \text{ mol mol}^{-1}$, where x'_i are the gas free liquid mole fractions. The number in parentheses indicates the uncertainty in the last digit.

These molecular models show mean unsigned deviations with respect to experimental data considering the whole temperature range from the triple point to the critical point of $\leq 1\%$ for the saturated liquid density and $\leq 5\%$ for the vapor pressure. Furthermore, the majority of these molecular models was assessed with respect to numerous other thermophysical properties, partly including transport data. Further details are given in the original publications.^{6,40–42}

To describe mixtures on the basis of pairwise additive potentials, molecular modeling reduces to specifying the interactions between unlike molecules. The unlike polar interactions were treated in a straightforward manner, following the laws of electrostatics without binary parameters. For the unlike LJ interactions, the modified Lorentz–Berthelot combination rule with one state-independent binary parameter ξ was used⁴³

$$\sigma_{AB} = (\sigma_A + \sigma_B)/2, \quad (3)$$

and

$$\varepsilon_{AB} = \xi \sqrt{\varepsilon_A \varepsilon_B}. \quad (4)$$

For the predictive mode, the binary parameter ξ was set to unity so that Eqs. (3) and (4) coincide with the Lorentz–Berthelot combination rule.⁴³ The resulting molecular mixture model is then based on pure fluid data alone.

For the adjusted mode, the binary parameter ξ was fitted to a single experimental vapor pressure of the mixture or a single Henry's law constant per binary system primarily in preceding work.^{6,7} In the present work, ξ was adjusted for the three binary subsystems oxygen + carbon dioxide, cyclohexane + cyclohexa-

nol, and cyclohexanone + cyclohexanol. Table 3 contains the experimental data which were used for the adjustment, the resulting binary parameter ξ , and the respective simulation results.

The Henry's law constant H_{ij} is related to the residual chemical potential μ_i^∞ of the solute i at infinite dilution in the solvent j by⁵⁰

$$H_{ij}(T, \mathbf{x}) = \rho_j RT \exp(\mu_i^\infty / (RT)), \quad (5)$$

where R is the gas constant and ρ_j is the molar density of the saturated liquid solvent. Molecular simulations to determine the Henry's law constant were carried out for all systems that contain one of the regarded gaseous components, that is, six binary systems, six ternary systems, and two quaternary systems. Furthermore, the pentenary system that contains both gaseous components was studied with respect to its vapor pressure, which was determined with the Grand Equilibrium method.⁵¹ The present numerical molecular simulation results are given in Supporting Information. The technical simulation details are summarized in the appendix.

COSMO-SAC

COSMO-SAC²³ yields the molar excess Gibbs free energy g^E on the basis of quantum mechanical solvation calculations. Because the studied fluid mixtures are compressible, these g^E data are supplied to a cubic EOS by means of the modified Huron–Vidal mixing rule. Here, the PRSV EOS³¹ was used, where pressure p , molar volume v and temperature T are inter-related by

$$p = \frac{RT}{v-b} - \frac{a}{v(v+b) + b(v-b)}. \quad (6)$$

The temperature-dependent energy parameter a is determined from the critical temperature T_c and the critical pressure p_c by

$$a = 0.45724 \frac{R^2 T_c^2}{p_c} \left[1 + \kappa \left(1 - \sqrt{\frac{T}{T_c}} \right) \right]^2, \quad (7)$$

with

$$\kappa = 0.378893 + 1.4897153 \omega - 0.17131848 \omega^2 + 0.0196654 \omega^3 + \kappa_1 \left(1 + \sqrt{\frac{T}{T_c}} \right) \left(0.7 - \frac{T}{T_c} \right), \quad (8)$$

where ω is the accentric factor. The volume parameter b was constant and given by

Table 3. Binary Parameter ξ of the Molecular Model, Binary Parameter l_{ij} of COSMO-SAC, Binary Parameter k_{ij} of the PR EOS, Experimental Vapor Pressure of the Mixture p^{exp} , or Henry's Law Constant H_{ij}^{exp} that was used for the Adjustment with Reference and Simulation Result with Adjusted ξ

Mixture (<i>i</i> + <i>j</i>)	ξ	l_{ij}	k_{ij}	T (K)	x_i (mol mol ⁻¹)	$p^{\text{exp}}/H_{ij}^{\text{exp}}$ (MPa)	$p^{\text{sim}}/H_{ij}^{\text{sim}}$ (MPa)
Oxygen + carbon dioxide	1	-0.0526	0.132	223.15	0.117	6.078 ⁴⁴	6.22 (6)
Oxygen + cyclohexane	0.90	-0.0547	0.22	313.15		79.5 ⁴⁵	79.6 (3)
Oxygen + cyclohexanone	0.93	-0.0342	0.355	313.15		161 ⁴⁶	159.9 (9)
Oxygen + cyclohexanol	0.91	-0.0266	0.345	313.6		201 (11) ⁷	194.1 (5)
Carbon dioxide + cyclohexane	0.95	-0.0523	0.217	313.15		16.2 ⁵	15.8 (4)
Carbon dioxide + cyclohexanone	0.985	-0.0082	0.049	313.15		8.5 ⁵	8.7 (9)
Carbon dioxide + cyclohexanol	0.918	-0.0418	0.225	313.6		27.1 (7) ⁷	27.8 (8)
Cyclohexane + cyclohexanone	0.982	-0.0228	0.065	348.15	0.442	0.058 ⁴⁷	0.058 (2)
Cyclohexane + cyclohexanol	0.982	-0.0035	0.07	308.15	0.529	0.0165 ⁴⁸	0.025 (1)
Cyclohexanone + cyclohexanol	1	-0.0027	0	383.15	0.55	0.022 ⁴⁹	0.023 (1)

The numbers in parentheses indicate the uncertainty in the last digits. x_i is specified if the vapor pressure was used, otherwise it was adjusted to the Henry's law constant.

$$b = 0.0778 \frac{RT_c}{p_c} \quad (9)$$

For describing mixtures, the first-order modified Huron–Vidal mixing rule³² is used

$$\frac{a}{bRT} = \sum_i x_i \frac{a_i}{b_i RT} - \frac{1}{0.53} \left[\frac{g^E}{RT} + \sum_i x_i \ln \left(\frac{b}{b_i} \right) \right], \quad (10)$$

and

$$b = \sum_i x_i b_i. \quad (11)$$

The excess Gibbs free energy g^E needed in the mixing rule (10) was obtained by COSMO-SAC

$$g^E = RT \sum_i x_i \ln \gamma_i, \quad (12)$$

where the activity coefficients γ_i are determined by

$$\ln \gamma_i = \left(\ln \frac{\Phi_i}{x_i} + \frac{z}{2} q_i \ln \frac{\Theta_i}{\Phi_i} + l_i - \frac{\Phi_i}{x_i} \sum_i x_i l_i \right) + \frac{A_i}{a_{\text{eff}}} \sum_s^{\text{NHB,OH,OT}} \sum_{\sigma_m} p_i^s(\sigma_m) [\ln \Gamma_M^s(\sigma_m) - \ln \Gamma_i^s(\sigma_m)]. \quad (13)$$

The term in brackets before the double summation in Eq. (13) is the Staverman–Guggenheim combinatorial model^{52,53} that accounts for molecular size and shape effects with

$$\Phi_i = \frac{x_i r_i}{\sum_i x_i r_i}, \quad \Theta_i = \frac{x_i q_i}{\sum_i x_i q_i}, \quad \text{and} \quad l_i = \frac{z}{2} (r_i - q_i) - (r_i - 1). \quad (14)$$

Therein, $z = 10$ is the coordination number, whereas r_i and q_i are the normalized volume and normalized surface area of component i , respectively. A_i is the surface area of component i and $a_{\text{eff}} = 7.25 \text{ \AA}^2$ is the effective segment area.²³

The σ -profile $p_i(\sigma)$ is a histogram of segments with the charge density σ on the molecular surface of component i . To achieve a better description of the hydrogen bonding interactions,^{54–56} the σ -profile is separated into three contributions

$$p_i(\sigma) = p_i^{\text{NHB}}(\sigma) + p_i^{\text{OH}}(\sigma) + p_i^{\text{OT}}(\sigma), \quad (15)$$

where $p_i^{\text{NHB}}(\sigma)$, $p_i^{\text{OH}}(\sigma)$, and $p_i^{\text{OT}}(\sigma)$ account for the segments of nonhydrogen bonding (NHB) atoms, hydroxyl (OH) groups, and other (OT) hydrogen bonding atoms (i.e., O, N, F, and H bound to N and F), respectively. The surface segments are, thus, also categorized into these three types. The σ -profiles of the five regarded components for the NHB, OH, and OT types are shown in Figure 1. The σ -profile is a species-specific property that can be seen as a fingerprint of a molecule. Because cyclohexane is composed of carbon and hydrogen atoms only, all its segments belong to the NHB type. Cyclohexanol has also segments of the OH type. The other three substances have also segments of the OT type. In case of cyclohexanol, the peaks on its NBH level are similar to those of cyclohexane, but its hydroxyl group leads to a strong polarity that can be seen as a large difference between minimum and maximum charge density of OH type. Cyclohexanol is the only molecule in this study that has a hydrogen bonding (proton) donor. For cyclohexanone, its σ -profile

of NHB type is slightly shifted toward negative charge densities, which shows that the oxygen atom in ketones has a strong effect on the surface charge distribution. It should be noted that a Gaussian-type function $\text{Prob}(\sigma) = 1 - \exp(\sigma^2/2\sigma_0^2)$ with $\sigma_0 = 0.007 \text{ e/\AA}^2$ is used in the current COSMO-SAC model to consider the probability of OH or OT segments to form hydrogen bonds. Therefore, only a small portion of the oxygen segments of oxygen and of carbon dioxide are collected on the OT level.

The σ -profile of the mixture M is obtained from

$$p_M^s(\sigma) = \frac{\sum_i x_i A_i p_i^s(\sigma)}{\sum_i x_i A_i}, \quad (16)$$

where the superscript $s = \text{NHB, OH, OT}$ indicates the surface segment type. $\Gamma_j^s(\sigma_m^s)$ is the activity coefficient of a type s segment with the charge density σ_m^s , where the subscript $j = i$ indicates a component and $j = M$ the mixture

$$\ln \Gamma_j^s(\sigma_m^s) = -\ln \left[\sum_t^{\text{NHB,OH,OT}} \sum_{\sigma_n^t} p_j^t(\sigma_n^t) \Gamma_j^s(\sigma_n^t) \exp \left(\frac{-\Delta W(\sigma_m^s, \sigma_n^t)}{RT} \right) \right]. \quad (17)$$

Therein, $\Delta W(\sigma_m^s, \sigma_n^t)$ is the electrostatic interaction between segment m (of type s) and segment n (of type t) with the charge densities σ_m^s and σ_n^t

$$\Delta W(\sigma_m^s, \sigma_n^t) = c_{\text{ES}}(\sigma_m^s + \sigma_n^t)^2 - c_{\text{HB}}(\sigma_m^s, \sigma_n^t)(\sigma_m^s - \sigma_n^t)^2, \quad (18)$$

with the temperature-dependent interaction coefficient $c_{\text{ES}}/(\text{kcal} \cdot \text{mol}^{-1} \text{ \AA}^4 \text{ e}^{-2}) = 6525.69 + 1.4859 \cdot 10^8/(T/K)^2$ and the hydrogen bonding coefficient

$$c_{\text{HB}}(\sigma_m^s, \sigma_n^t)/(\text{kcal} \cdot \text{mol}^{-1} \text{ \AA}^4 \text{ e}^{-2}) = \begin{cases} 4013.78 & \text{if } s = t = \text{OH} \text{ and } \sigma_m^s \cdot \sigma_n^t < 0, \\ 932.31 & \text{if } s = t = \text{OT} \text{ and } \sigma_m^s \cdot \sigma_n^t < 0, \\ 3016.43 & \text{if } s = \text{OH}, t = \text{OT} \text{ and } \sigma_m^s \cdot \sigma_n^t < 0, \\ 0 & \text{otherwise.} \end{cases} \quad (19)$$

These global parameter values were taken from Ref. 23 without further adjustment. More details of the COSMO-SAC model can be found in the literature.²³

In the predictive mode, which is the usual COSMO approach, Eqs. (6)–(19) rely exclusively on experimental pure fluid data that are needed to parameterize the PRSV EOS. The mixture behavior is described via g^E data that stem from predictive quantum chemical solvation calculations. The results obtained with the PRSV EOS³¹ in combination with the first-order modified Huron–Vidal mixing rule³² and COSMO-SAC²³ are referred to as COSMO-SAC in the following.

For the adjusted mode, one state-independent binary parameter l_{ij} was introduced into the volume parameter b of the first-order modified Huron–Vidal mixing rule.³² Equation (11) was changed in this case to

$$b = \sum_i \sum_j x_i x_j \frac{b_i + b_j}{2} (1 - l_{ij}). \quad (20)$$

The binary parameter l_{ij} was fitted to the same experimental binary vapor pressure or Henry's law constant data as the binary parameter ξ of the molecular force field models described above, compared in Table 3.

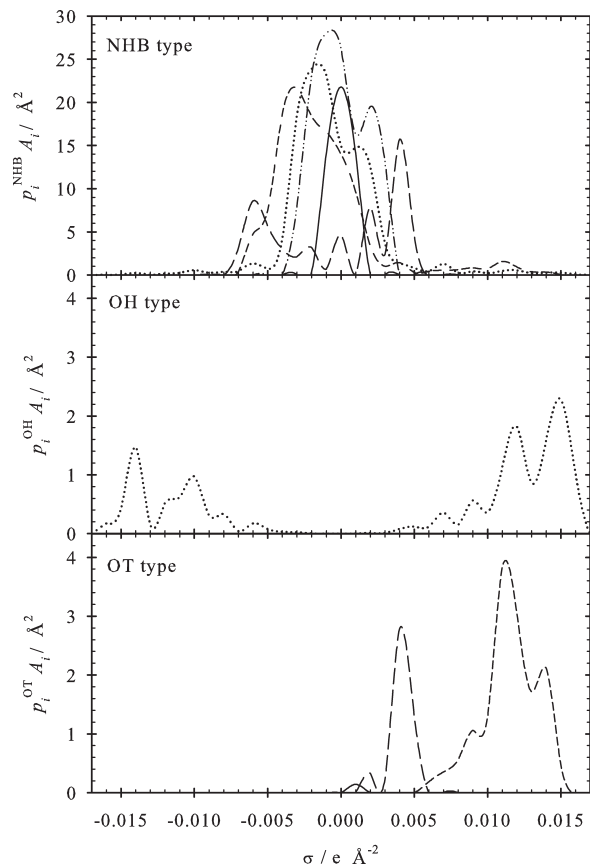


Figure 1. The σ -profiles of the five regarded components of NHB type (top), OH type (center), and OT type (bottom): — oxygen; — — carbon dioxide; - ... cyclohexane; - - cyclohexanone; ... cyclohexanol.

For the present calculations of the Henry's law constant with COSMO-SAC, the same procedure was applied as for the determination of the Henry's law constant from experimental data, with the difference that also the vapor phase fugacity was taken from COSMO-SAC.

Peng–Robinson Equation of State

The original PR EOS¹⁸ with the simple van der Waals mixing rule was considered as a cubic EOS baseline. It is defined by Eqs. (6)–(9), but it has an acentric factor polynomial κ that is simpler than Eq. (8)

$$\kappa = 0.37464 + 1.54226 \omega - 0.26992 \omega^2. \quad (21)$$

The van der Waals mixing rule defines the temperature-dependent energy parameter as

$$a = \sum_i \sum_j x_i x_j a_{ij}, \quad (22)$$

with

$$a_{ij} = \sqrt{a_{ii} a_{jj}} (1 - k_{ij}). \quad (23)$$

Therein, k_{ij} is an adjustable binary parameter that was fitted to the same experimental binary data as all other models in the adjusted mode, compared in Table 3. For the predictive mode, $k_{ij} = 0$. The constant volume parameter b was defined as usual according to Eq. (11).

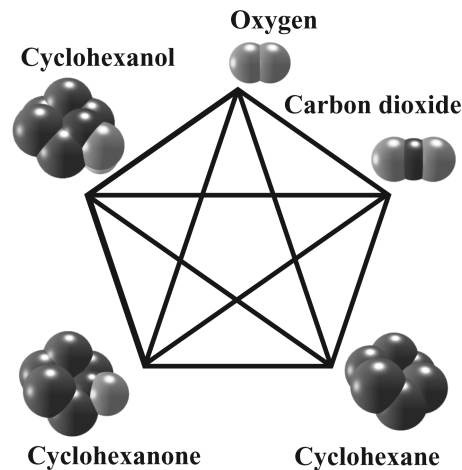


Figure 2. Schematic of the pentenary mixture and its binary subsystems together with snapshots of the employed molecular models.

Results and Discussion

Binary subsystems

All 10 binary subsystems that can be formed from the regarded five components were investigated here. Figure 2 shows a schematic of these binary subsystems along with snapshots of the employed molecular models. Because of the pairwise treatment of the molecular interactions by all approaches that were studied here, knowledge on the binary subsystems is crucial for the multicomponent systems. A good match of the binary phase behavior is a prerequisite for good predictions in case of higher order systems.

For all binary subsystems, results from molecular simulation, COSMO-SAC, and the PR EOS were compared to experimental data from the literature. Critical temperature T_c , critical pressure p_c , acentric factor ω , and κ_1 used for the PR EOS and the PRSV EOS are listed in Table 4.

Molecular simulation, COSMO-SAC, and the PR EOS were applied in two different modes: (1) strictly predictive, that is, $\xi = 1$, $l_{ij} = 0$, and $k_{ij} = 0$, and, if necessary, (2) adjusted to a single experimental binary data point. The PR EOS results in the predictive mode were omitted in the figures discussed below to avoid visual clutter and because they are inferior. Supporting Information contains plots with these data. Note that the same experimental binary data were used for the adjustment of all binary parameters to achieve a fair comparison, compared in Table 3. The single experimental binary data point was chosen to be around 313 K in case of Henry's law constant and near the equimolar composition in case of VLE.

With respect to VLE data, two isotherms with a temperature difference of 20–120 K are presented. The Henry's law constant was studied over a temperature range of about 120 K.

Oxygen + carbon dioxide

The VLE of oxygen + carbon dioxide is presented in Figure 3 for the two isotherms 223.15 and 273.15 K. Oxygen is supercritical for both temperatures so that the saturated liquid line has a typical concave shape. The present molecular simulation results, which are predictive with $\xi = 1$, are in very good agreement with the experimental data⁴⁴ almost in the entire studied range. Only near the critical region of the

Table 4. Critical Temperature T_c , Critical Pressure p_c , Acentric Factor ω , and Vapor Pressure Parameter κ_1 used in the Present Work for the PR EOS and the PRSV EOS

Component	T_c (K)	p_c (MPa)	ω	κ_1
Oxygen	154.77 ³¹	5.09 ³¹	0.02128 ³¹	0.01512 ³¹
Carbon dioxide	304.21 ⁵⁷	7.382 ⁵⁷	0.225 ⁵⁷	0.04285 ⁵⁷
Cyclohexane	553.64 ⁵⁷	4.075 ⁵⁷	0.20877 ⁵⁷	0.07023 ⁵⁷
Cyclohexanone	653 ⁵⁸	4.0 ⁵⁸	0.299006 ⁵⁸	0.0435
Cyclohexanol	650.1 ⁵⁸	4.26 ⁵⁸	0.369047 ⁵⁸	0.5682

The vapor pressure parameter κ_1 for cyclohexanone and cyclohexanol was fitted in the present work to experimental vapor pressure data compiled by DIPPR.⁵⁸

mixture, the simulation results overpredict the vapor pressure and the oxygen content of the saturated vapor phase. Compared to the adjusted PR EOS, the simulation results show a better agreement with the experiment near the critical region of the mixture. Predictions by COSMO-SAC show a vapor pressure that is significantly too low for both temperatures; however, the vapor phase composition is in very good agreement with the experiment. In adjusted mode ($l_{ij} = -0.0526$), COSMO-SAC is as good as molecular simulation, except for the extended critical region.

Oxygen + cyclohexane, oxygen + cyclohexanone, and oxygen + cyclohexanol

Due to the large difference in terms of the volatility between oxygen and the cyclic compounds, exclusively data on the Henry's law constant are available in the literature^{7,45,46,59-61} for oxygen + cyclohexane, oxygen + cyclohexanone, and oxygen + cyclohexanol, compared in Figure 4. With an adjusted binary parameter ($\xi = 0.91, 0.93,$ and 0.90), the molecular simulation results are in excellent agreement with the experiment^{7,45,46,59-61} for all three systems throughout the entire temperature range for which experimental data are available. COSMO-SAC underpredicts the Henry's

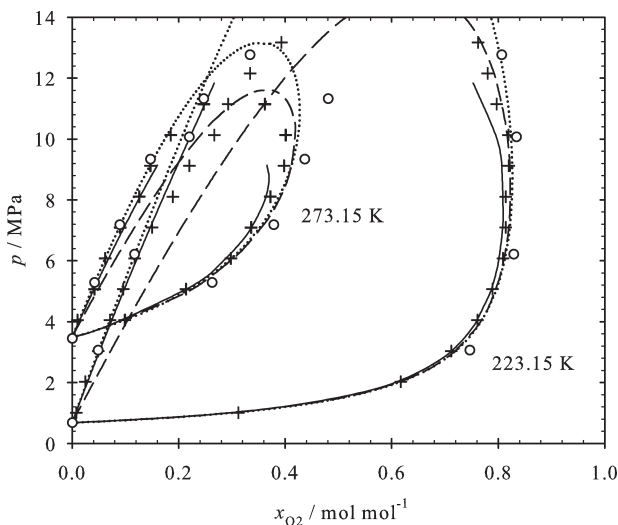


Figure 3. Isothermal vapor-liquid phase diagram of oxygen + carbon dioxide at 223.15 and 273.15 K: + experimental data⁴⁴; ○ present simulation data with $\xi = 1$; - - COSMO-SAC; — COSMO-SAC with $l_{ij} = -0.0526$; ... PR EOS with $\kappa_{ij} = 0.132$.

The statistical simulation uncertainties are within symbol size.

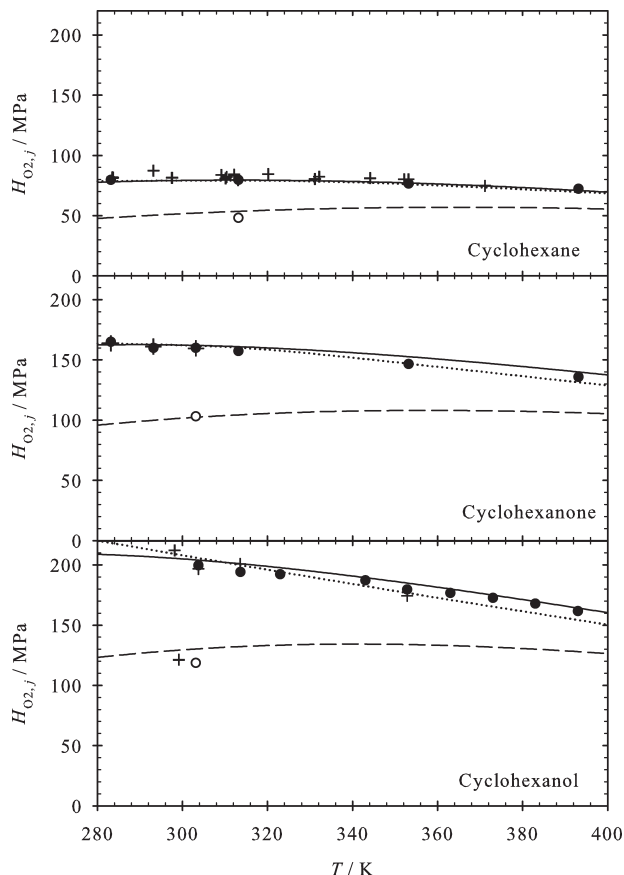


Figure 4. From top to bottom: Henry's law constant of oxygen in cyclohexane, in cyclohexanone, and in cyclohexanol: + experimental data^{5,7,45,46,59-61}; ○ present simulation data with $\xi = 1$; ● present simulation data with $\xi = 0.91, 0.93,$ and 0.90 ; - - COSMO-SAC; — COSMO-SAC with $l_{ij} = -0.0547, -0.0342,$ and -0.0266 ; ... PR EOS with $\kappa_{ij} = 0.22, 0.255,$ and 0.345 .

The statistical simulation uncertainties are within symbol size.

law constant with a maximum deviation of around 55% at low temperatures. However, molecular simulation in predictive mode ($\xi = 1$) is similarly far off. The agreement of the adjusted COSMO-SAC model ($l_{ij} = -0.0547, -0.0342,$ and -0.0266) with the experimental data is excellent as well. The adjusted PR EOS yields similarly good results. Note that the single experimental data point by Cauquil⁶¹ for oxygen + cyclohexanol ($H_{O_2,j} = 121.3$ MPa at 299.15 K) was not confirmed in a previous work⁷ and is shown here for completeness only.

Carbon dioxide + cyclohexane, carbon dioxide + cyclohexanone, and carbon dioxide + cyclohexanol

VLE of the binary systems carbon dioxide + cyclohexane, carbon dioxide + cyclohexanone, and carbon dioxide + cyclohexanol as well as the Henry's law constant of carbon dioxide in cyclohexane, in cyclohexanone, and in cyclohexanol are presented in Figures 5–8. For these three binary systems, all models were adjusted to the Henry's law constant, compared in Table 3. Molecular simulation and COSMO-SAC (both in adjusted mode) show a similar agreement with

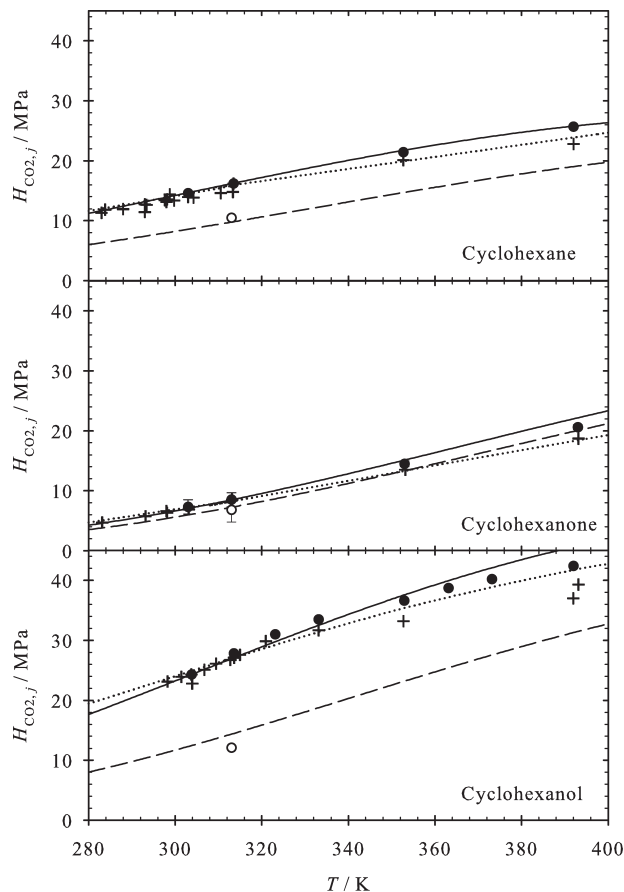


Figure 5. From top to bottom: Henry's law constant of carbon dioxide in cyclohexane, in cyclohexanone, and in cyclohexanol: + experimental data^{5,7,45,46,63-67}; ○ present simulation data with $\xi = 1$; ● simulation data with $\xi = 0.95$, 0.985, and 0.918^{6,7}; - - - COSMO-SAC; - COSMO-SAC with $l_{ij} = -0.0523$, -0.0082 , and -0.0418 ; ... PR EOS with $k_{ij} = 0.217$, 0.049, and 0.225.

The statistical simulation uncertainties are not shown if they are within symbol size.

the experimental data^{5,7,45,46,63-67} for $H_{CO_2,j}$ of these systems, compared in Figure 5. The agreement is excellent at lower temperatures, but at higher temperatures they overpredict. The adjusted PR EOS describes the Henry's law constant best for these three systems. The predictions by molecular simulation and COSMO-SAC are similarly far off.

Figure 6 presents the VLE of carbon dioxide + cyclohexane. In adjusted mode, molecular simulation ($\xi = 0.95$) and COSMO-SAC ($l_{ij} = -0.0523$) are in good agreement with the experimental data^{5,8} at 313.15 K. However, at 410.9 K, both predict a higher vapor pressure than the experiment.⁶⁸ Predictions by molecular simulation and COSMO-SAC show a similarly too low vapor pressure at 313.15 K. The PR EOS, which was adjusted to the Henry's law constant ($k_{ij} = 0.217$), has difficulties in describing the VLE at 313.15 K. At 410.9 K, the PR EOS yields a similarly high vapor pressure as the two other models. None of the studied theoretical approaches is capable to cover both temperatures consistently for this system with a state-independent adjustable parameter.

With respect to the VLE of carbon dioxide + cyclohexanone, all models are at least in good agreement with the

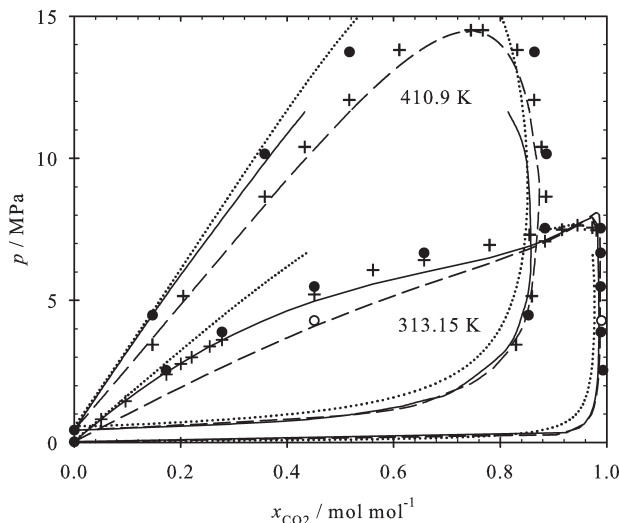


Figure 6. Isothermal vapor-liquid phase diagram of carbon dioxide + cyclohexane at 313.15 and 410.9 K: + experimental data^{5,8,68}; ○ present simulation data with $\xi = 1$; ● simulation data with $\xi = 0.95$ ⁶; - - COSMO-SAC; - COSMO-SAC with $l_{ij} = -0.0523$; ... PR EOS with $k_{ij} = 0.217$.

The statistical simulation uncertainties are within symbol size.

experimental data^{5,8,69,70} at 313.15 K, compared in Figure 7. Molecular simulation, the PR EOS (both adjusted), and the predictions by COSMO-SAC yield a too high vapor pressure only near the critical point of the mixture at the high temperature (433.5 K). Molecular simulation in predictive mode yields a somewhat too low vapor pressure. Overall, the predictions by COSMO-SAC are in good agreement with the experimental data also for the high temperature.

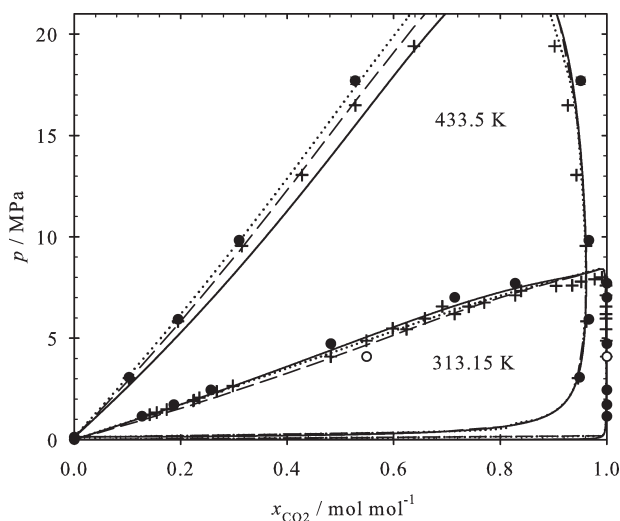


Figure 7. Isothermal vapor-liquid phase diagram of carbon dioxide + cyclohexanone at 313.15 and 433.5 K: + experimental data^{5,8,69,70}; ○ present simulation data with $\xi = 1$; ● simulation data with $\xi = 0.985$ ⁶; - - COSMO-SAC; - COSMO-SAC with $l_{ij} = -0.0082$; ... PR EOS with $k_{ij} = 0.049$.

The statistical simulation uncertainties are within symbol size.

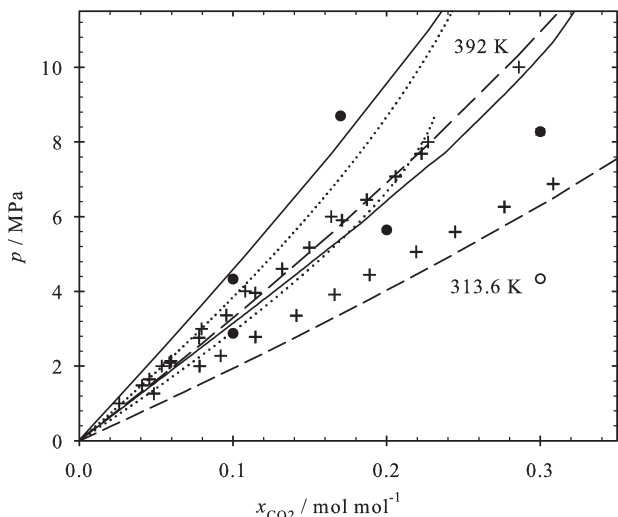


Figure 8. Isothermal vapor-liquid phase diagram (saturated liquid line only) of carbon dioxide + cyclohexanol at 313.6 and 392 K: + experimental data^{5,62}; o present simulation data with $\xi = 1$; • simulation data with $\xi = 0.918$ ⁶; - - COSMO-SAC; — COSMO-SAC with $l_{ij} = -0.0418$; ... PR EOS with $k_{ij} = 0.225$.

The statistical simulation uncertainties are within symbol size.

VLE data for carbon dioxide + cyclohexanol at 313.6 and 392 K are shown in Figure 8. None of the models is capable to accurately cover the VLE of this system, where it should be pointed out that the binary parameters were adjusted to the Henry's law constant. The discrepancies are particularly astonishing for 313 K as the Henry's law constant for that temperature is well-described by the models. The available VLE data are not in contradiction with the Henry data, but show strong deviations from Henry's law already at low finite concentrations. This may be attributed to the existence of a liquid-liquid equilibrium for this system, as shown by Esmelindro et al.⁸ The best results were obtained by COSMO-SAC in predictive mode, followed by molecular simulation in adjusted mode ($\xi = 0.918$). Adjusted COSMO-SAC ($l_{ij} = -0.0418$) and the adjusted PR EOS ($k_{ij} = 0.225$) are similarly far off from the experiment. Predictive molecular simulation shows a too low vapor pressure at 313 K.

Cyclohexane + cyclohexanone

VLE data of cyclohexane + cyclohexanone are shown in Figure 9 at 323.15 and 348.15 K. Molecular simulation ($\xi = 0.982$), COSMO-SAC ($l_{ij} = -0.0228$), and the PR EOS ($k_{ij} = 0.065$), all in adjusted mode, are throughout in very good agreement with the experimental data.⁴⁷ COSMO-SAC slightly underpredicts the vapor pressure. The same deviation was found for the predictive simulation results.

Cyclohexane + cyclohexanol

Comparisons for the VLE of this system are shown for the two temperatures 308.15 and 328.15 K in Figure 10. Note that the same binary parameter of the molecular model, i.e., $\xi = 0.982$, as for the system cyclohexane + cyclohexanone was obtained from the adjustment. The present simulation results and COSMO-SAC are in very good agreement with the experimental data.⁴⁸ The PR EOS with $k_{ij} = 0.07$ leads

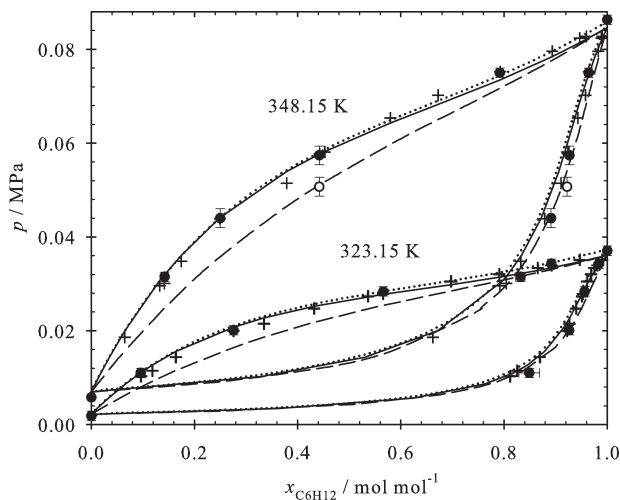


Figure 9. Isothermal vapor-liquid phase diagram of cyclohexane + cyclohexanone at 323.15 and 348.15 K: + experimental data⁴⁷; o present simulation data with $\xi = 1$; • simulation data with $\xi = 0.98$ ⁶; - - COSMO-SAC; — COSMO-SAC with $l_{ij} = -0.0228$; ... PR EOS with $k_{ij} = 0.065$.

to a qualitatively wrong S-shaped slope of the saturated liquid line, which can particularly well be seen at 328.15 K. Molecular simulation slightly overpredicts the vapor pressure at 303.15 K. In adjusted mode ($l_{ij} = -0.0035$), COSMO-SAC only slightly better describes the experimental data.⁴⁸

Cyclohexanone + cyclohexanol

Figure 11 shows the VLE of cyclohexanone + cyclohexanol at 353.15 and 383.15 K. As for oxygen + carbon dioxide, the simulation results in predictive mode are in excellent agreement with the experiment. Only a single VLE simulation point shows significant deviations for vapor pressure or

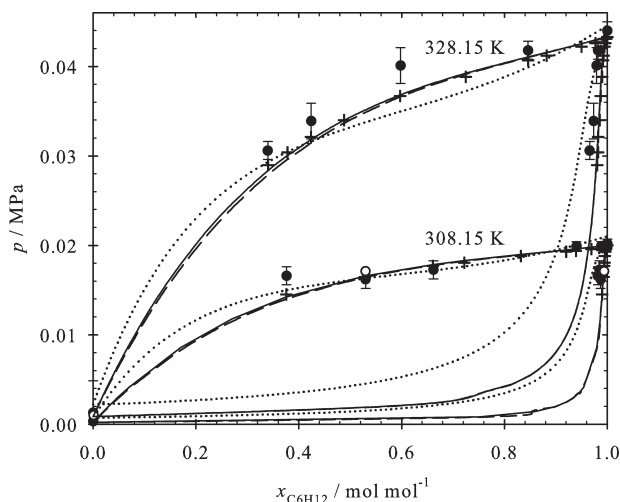


Figure 10. Isothermal vapor-liquid phase diagram of cyclohexane + cyclohexanol at 308.15 and 328.15 K: + experimental data⁴⁸; o present simulation data with $\xi = 1$; • present simulation data with $\xi = 0.982$; - - - COSMO-SAC; — COSMO-SAC with $l_{ij} = -0.0035$; ... PR EOS with $k_{ij} = 0.07$.

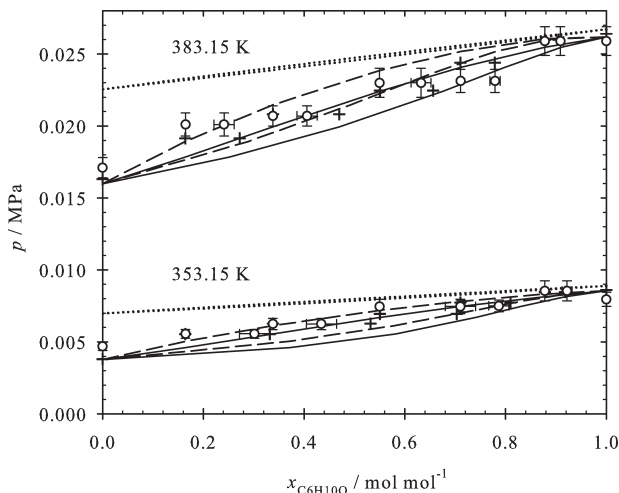


Figure 11. Isothermal vapor-liquid phase diagram of cyclohexanone + cyclohexanol at 353.15 and 383.15 K: + experimental data⁴⁹; ○ present simulation data with $\xi = 1$; - - - COSMO-SAC; — COSMO-SAC with $I_{ij} = -0.0027$; ... PR EOS with $k_{ij} = 0$.

vapor phase composition. These discrepancies are due to sampling problems at the regarded temperatures that are not very far from the triple point of both components. The PR EOS is not capable to describe the VLE, because the vapor pressure of pure cyclohexanol is poorly represented. A very good agreement with the experimental data⁴⁹ was found for molecular simulation in predictive mode. COSMO-SAC in adjusted mode ($I_{ij} = -0.0027$) yields a somewhat too low vapor pressure, whereas in predictive mode it is too high.

In addition, the isobaric VLE at 0.066 MPa was studied for this system, see Figure 12. A very good agreement of the predictive simulation data with the experiment was found throughout. COSMO-SAC shows some deviations and yields in predictive mode an azeotropic point which was not observed by experiment,⁷¹ simulation, or adjusted COSMO-SAC. The PR EOS is again not capable to describe the vapor pressure of the pure components. Here, the difference between the PR EOS and the PRSV EOS (which is part of COSMO-SAC) becomes visible. The acentric factor polynomial κ of the PRSV EOS was adjusted to several experimental pure substance vapor pressure data points, compared in Eqs. (8) and (21).

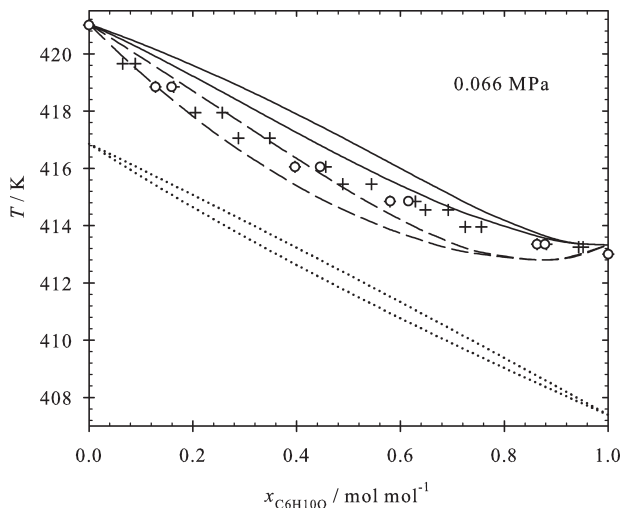


Figure 12. Isobaric vapor-liquid phase diagram of cyclohexanone + cyclohexanol at 0.066 MPa: + experimental data⁷¹; ○ present simulation data with $\xi = 1$; - - - COSMO-SAC; — COSMO-SAC with $I_{ij} = -0.0027$; ... PR EOS with $k_{ij} = 0$.

The statistical simulation uncertainties are within symbol size.

Overview

In the present work, 10 binary systems were studied with three different models and two types of data (VLE and Henry's law constant) were considered. To give an overview on the results of the comparison of the models with the data is not trivial. We have decided to try to do this using an empirical classification of the quality of the representation simply by --, -, 0, + and ++, which corresponds to 0–4 points, compared in Table 5. The score -- means that the approach does not agree with the experimental data at all and ++ means that this agreement is very good. If both VLE data and Henry's law constant data were available for a mixture, the mean score was assigned. We have not used quantitative criteria for the classification, but rather the impression from assessing the results in Figures 3–12.

Table 5 additionally shows the score for the PR EOS in predictive mode, which was excluded in the figures and the discussion above due to its inferior performance. Note that these data are presented in the Supporting Information. The PR EOS

Table 5. Scores of the Studied Modeling Approaches to Predict and Describe Fluid-Phase Coexistence Data for the Binary Mixtures

Mixture	Molecular Simulation		COSMO-SAC		Peng-Robinson EOS	
	Predictive	Adjusted	Predictive	Adjusted	Predictive	Adjusted
Oxygen + carbon dioxide	++	++	-	++	-	++
Oxygen + cyclohexane	-	++	-	++	-	++
Oxygen + cyclohexanone	-	++	-	++	--	++
Oxygen + cyclohexanol	-	++	-	++	--	++
Carbon dioxide + cyclohexane	-	+	-	+	--	0
Carbon dioxide + cyclohexanone	+	++	+	++	0	++
Carbon dioxide + cyclohexanol	-	+	0	+	--	0
Cyclohexane + cyclohexanone	0	++	0	++	-	++
Cyclohexane + cyclohexanol	++	++	++	++	--	0
Cyclohexanone + cyclohexanol	++	++	0	+	--	--
Final score	22	38	18	37	5	30

The scale ranges from --, -, 0, +, and ++ which corresponds to 0–4 points, respectively.

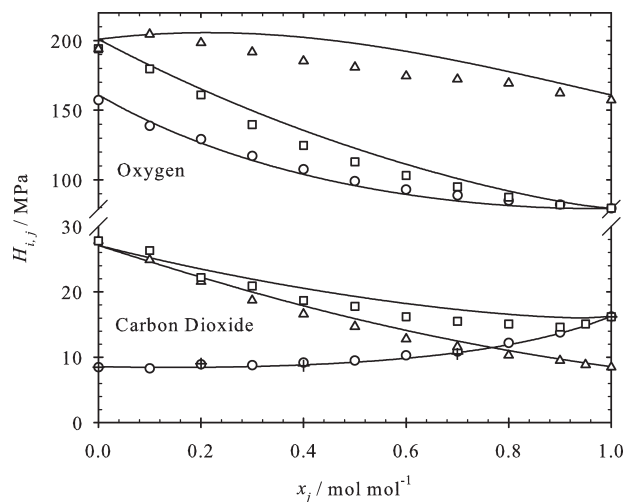


Figure 13. Henry's law constant from present simulations of oxygen (top) and of carbon dioxide (bottom) at 313.6 K in binary liquid mixtures of: ○ cyclohexane + cyclohexanone plotted over the cyclohexane mole fraction; □ cyclohexane + cyclohexanol plotted over the cyclohexane mole fraction; Δ cyclohexanone + cyclohexanol plotted over the cyclohexanone mole fraction; + experimental data⁵; — COSMO-SAC.

The statistical simulation uncertainties are within symbol size.

in predictive mode has by far the lowest score with 5 points, because the predictions show a too ideal behavior in general. COSMO-SAC in predictive mode has a score of 18 points, followed by molecular simulation in predictive mode with 22 points. The difference of 4 points is due to the better description of oxygen + carbon dioxide and cyclohexanone + cyclohexanol. Otherwise, these two predictive methods showed a similar performance. The adjusted PR EOS achieved 30 points and is clearly better than the predictive approaches, but significantly worse than molecular simulation and COSMO-SAC in adjusted mode with 38 and 37 points, respectively.

The effort that is associated with the determination of one Henry's law constant value on the basis of calibrated laboratory equipment was around 4 working days. Molecular simulation required 6 h and COSMO-SAC around 15 min.

Due to its inferior performance for the binary subsystems, the PR EOS was excluded from the study of the higher order systems that are discussed in the following sections.

Ternary Subsystems

Among the 10 possible combinations to form a ternary mixture from five components, six were selected. These are the ternary systems containing one of the gaseous components (oxygen or carbon dioxide) and two of the three solvents (cyclohexane, cyclohexanone, or cyclohexanol). The study was carried out by molecular simulation and COSMO-SAC²³ in terms of the Henry's law constant of the gaseous component at 313.6 K. Unfortunately, experimental data were available only for carbon dioxide in cyclohexane + cyclohexanone. The models were considered in adjusted mode only, that is, with ζ and l_{ij} fitted to

binary experimental data, compared in Table 3. In Figure 13, the Henry's law constant of both gases in all three binary subsystems of cyclohexane + cyclohexanone + cyclohexanol is presented.

Oxygen in binary mixtures

For the Henry's law constant of oxygen in mixtures of cyclohexane + cyclohexanone, the main variation occurs at low cyclohexane mole fractions. At high cyclohexane mole fractions, the slope of $H_{O_2,j}$ flattens. The predictions by molecular simulation and COSMO-SAC agree very well.

For the Henry's law constant of oxygen in mixtures of cyclohexane + cyclohexanol, the same qualitative behavior as for the system cyclohexane + cyclohexanone was found; the Henry's law constant varies most at low cyclohexane mole fractions. COSMO-SAC predicts a more ideal behavior than molecular simulation.

In case of the Henry's law constant of oxygen in mixtures of cyclohexanone + cyclohexanol, a qualitatively different behavior was found. The Henry's law constant from molecular simulation decreases almost linearly on addition of cyclohexanone to cyclohexanol in most of the composition range. Molecular simulation predicts a little pronounced maximum at a cyclohexanone mole fraction of around 0.1 mol mol⁻¹. COSMO-SAC predicts a maximum as well, but at a somewhat different composition.

Carbon dioxide in binary mixtures

The Henry's law constant of carbon dioxide in cyclohexane + cyclohexanone varies strongly on addition of small amounts of cyclohexanone to pure cyclohexane, whereas at lower cyclohexane mole fractions, it remains almost unchanged. Molecular simulation and COSMO-SAC yield very similar results for this ternary system and are in very good agreement with that experimental data.⁵

The Henry's law constant of carbon dioxide in cyclohexane + cyclohexanol decreases on addition of cyclohexane to pure cyclohexanol. The molecular simulation data exhibit a minimum at a cyclohexane mole fraction of around 0.9 mol mol⁻¹. COSMO-SAC does not predict a minimum, but a monotonous decrease.

In case of carbon dioxide in cyclohexanone + cyclohexanol, a similar behavior as in cyclohexane + cyclohexanol was observed, except that no minimum was predicted. The Henry's law constant varies less on addition of cyclohexanol to pure cyclohexanone, whereas it varies more on addition of cyclohexanone to pure cyclohexanol. COSMO-SAC and molecular simulation yield again similar results.

Quaternary and Pentenary Systems

Gas solubility measurements

The solubility pressure of pure carbon dioxide (1) and of pure oxygen (2) as well as of their gaseous mixture in the ternary solvent mixture cyclohexane (3) + cyclohexanone (4) + cyclohexanol (5) was determined in this work by experiment at 313.6 K for total pressures of up to 8.8 MPa, compared in Table 1. Two solvent mixture compositions were measured: Mixture A, nearly equimolar ($x'_3 = 0.325$ mol mol⁻¹, $x'_4 = 0.35$ mol mol⁻¹, $x'_5 = 0.325$ mol mol⁻¹) and Mixture B, rich in cyclohexane with almost the same mole fractions of cyclohexanone and cyclohexanol ($x'_3 = 0.764$ mol mol⁻¹, $x'_4 = 0.119$ mol mol⁻¹,

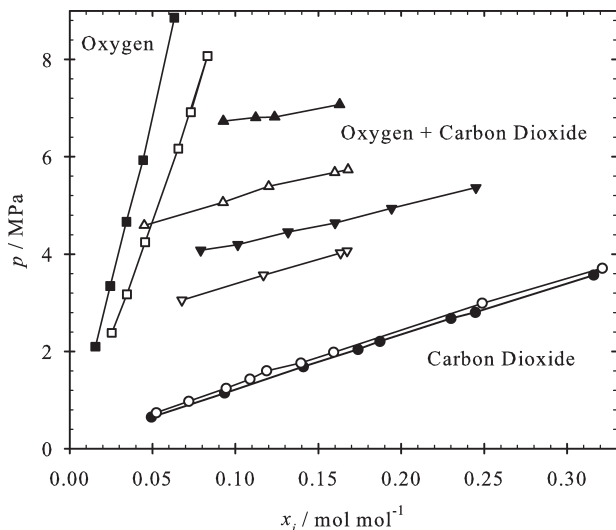


Figure 14. Solubility pressure of oxygen (1), carbon dioxide (2), and mixtures of the two gases in two ternary [cyclohexane (3), cyclohexanone (4), and cyclohexanol (5)] solvent mixtures A (full symbols) and B (open symbols) at 313.6 K from present experiments: Mixture A: $x'_3 = 0.325 \text{ mol mol}^{-1}$, $x'_4 = 0.35 \text{ mol mol}^{-1}$, $x'_5 = 0.325 \text{ mol mol}^{-1}$. Mixture B: $x'_3 = 0.764 \text{ mol mol}^{-1}$, $x'_4 = 0.119 \text{ mol mol}^{-1}$, $x'_5 = 0.117 \text{ mol mol}^{-1}$: ■, □ pure oxygen ($x_i = x_{\text{O}_2}$); ●, ○ pure carbon dioxide ($x_i = x_{\text{CO}_2}$); ▼, ▽ carbon dioxide ($x_i = x_{\text{CO}_2}$), and a constant liquid mole fraction of oxygen of $x'_{\text{O}_2} = 0.02 \text{ mol mol}^{-1}$; ▲, △ carbon dioxide ($x_i = x_{\text{CO}_2}$) and a constant liquid mole fraction of oxygen of $x'_{\text{O}_2} = 0.04 \text{ mol mol}^{-1}$; — guide for the eye.

The uncertainties of all data are within symbol size.

$x'_5 = 0.117 \text{ mol mol}^{-1}$), where x'_i denotes the gas free liquid mole fraction of component i . Note that Esmelindro et al.⁸ have studied mixture A as well. The present experimental data are plotted in Figure 14. In case of oxygen, the solubility decreases from mixture A to B, whereas in case of carbon dioxide, it slightly increases.

The studied pentenary mixture was based on the ternary liquid solvent mixtures A and B. By adding oxygen, quaternary mixtures with $x'_{\text{O}_2} = 0.02$ and $0.04 \text{ mol mol}^{-1}$ were prepared. Subsequently, carbon dioxide was introduced to form the pentenary mixture with a varying carbon dioxide mole fraction. A linear increase of the solubility pressure on addition of carbon dioxide was observed, compared in Figure 14. The solubility pressure decreases more in mixture A than in mixture B. The difference is more dominant for the (carbon dioxide free) oxygen mole fraction of $x'_{\text{O}_2} = 0.04 \text{ mol mol}^{-1}$ than for $x'_{\text{O}_2} = 0.02 \text{ mol mol}^{-1}$.

The present experimental results for mixture A are compared in Figure 15 to experimental data by Esmelindro et al.,⁸ to simulation results, and to COSMO-SAC (both adjusted to binary experimental data). For the pure gases, a good agreement was found with both the experimental data by Esmelindro et al.⁸ and the present theoretical models. Overall, the simulation results and COSMO-SAC also agree very well with the present experimental data for the penta-

nary mixture. Note that analogous data for mixture B, that lead to the same conclusions, are not shown.

Henry's law constant

The present experimental Henry's law constant data of oxygen in the two ternary liquid solvent mixtures A and B are compared to molecular simulation and COSMO-SAC in Figure 16. Again, the agreement between present data from experiment, simulation, and COSMO-SAC is very good. For the molecular simulations and COSMO-SAC, the dependence of the Henry's law constant of oxygen on the cyclohexane mole fraction (cyclohexanone and cyclohexanol were kept equimolar) was studied. The Henry's law constant of oxygen varies most strongly on addition of cyclohexane to the equimolar mixture cyclohexanone + cyclohexanol. At high cyclohexane mole fractions, the decrease of the Henry's law constant is less pronounced. COSMO-SAC predicts a higher Henry's law constant at low cyclohexane mole fractions.

Analogously, the dependence of the Henry's law constant of carbon dioxide on the cyclohexane mole fraction (cyclohexanone and cyclohexanol were kept equimolar) is shown in Figure 16. Only a weak influence was found. Starting from the Henry's law constant of carbon dioxide in

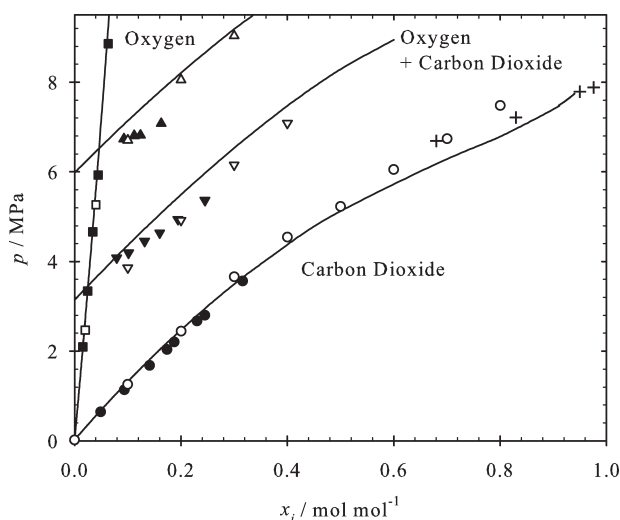


Figure 15. Solubility pressure of oxygen (1) and of carbon dioxide (2) in the ternary [cyclohexane (3), cyclohexanone (4), and cyclohexanol (5)] solvent mixture A with $x'_3 = 0.325 \text{ mol mol}^{-1}$, $x'_4 = 0.35 \text{ mol mol}^{-1}$, $x'_5 = 0.325 \text{ mol mol}^{-1}$ at 313.6 K. Pure carbon dioxide: ● present experimental data; + experimental data by Esmelindro et al.⁸ Pure oxygen: ■ present experimental data. Carbon dioxide at a constant liquid mole fraction of oxygen of $x'_{\text{O}_2} = 0.02 \text{ mol mol}^{-1}$: ▼ present experimental data. Carbon dioxide at a constant liquid mole fraction of oxygen of $x'_{\text{O}_2} = 0.04 \text{ mol mol}^{-1}$: ▲ present experimental data. Open symbols depict the present simulation data. — COSMO-SAC.

The uncertainties of the data are mostly within symbol size.

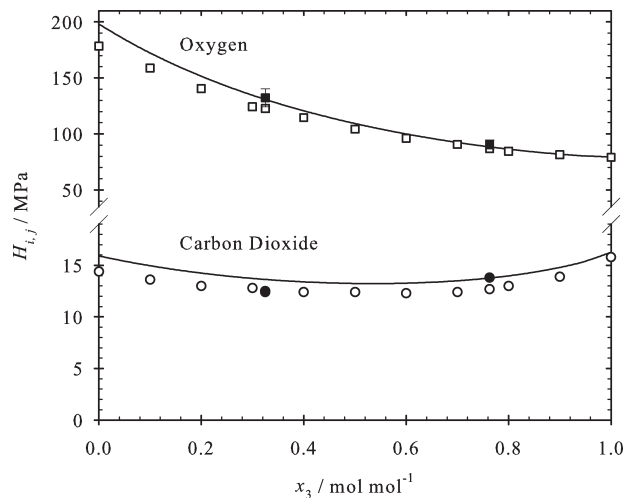


Figure 16. Henry's law constant of either \blacksquare oxygen (1) or \bullet carbon dioxide (2) in the ternary mixture of cyclohexane (3) + cyclohexanone (4) + cyclohexanol (5) at 313.6 K. The gas free composition of the solvent is varied so that $x'_4 = x'_5$, where $x'_4 = x'_5 = 1 - x'_3$: (full symbols) present experimental data; (open symbols) present simulation data; — COSMO-SAC.

The uncertainties of the present data are not shown if they are within symbol size.

equimolar cyclohexanone + cyclohexanol, the Henry's law constant decreases slightly on addition of cyclohexane until a minimum is reached at a cyclohexane mole fraction of around 0.5 mol mol⁻¹. COSMO-SAC predicts a somewhat higher Henry's law constant than molecular simulation, but both agree well with the experiment.

Conclusions

Three theoretical approaches, that is, molecular simulation, COSMO-SAC, and the PR EOS, were assessed in a comprehensive study with respect to their predictive and descriptive capabilities for fluid-phase coexistence data of an industrially important pentenary mixture. For binary data, the PR EOS in predictive mode has by far the poorest performance. Molecular simulation and COSMO-SAC in predictive mode are much better. The PR EOS in adjusted mode is satisfying for most of the 10 binary subsystems, but shows a qualitatively wrong description of carbon dioxide + cyclohexane, carbon dioxide + cyclohexanol, and cyclohexanone + cyclohexanol. The best performance was achieved with molecular simulation and COSMO-SAC in adjusted mode. Both methods are capable to describe the experimental data over a wide range of states with an accuracy that is well-suitable for industrial applications.

For the six studied ternary subsystems, molecular simulation and COSMO-SAC showed a similar performance with respect to the prediction of the Henry's law constant of pure carbon dioxide and of pure oxygen in all three binary solvent mixtures containing cyclohexane, cyclohexanone, or cyclohexanol. Both methods predicted the same composition dependence of the Henry's law constant. A clear advantage of one method over the other was not found.

Predictions by molecular simulation and COSMO-SAC for two quaternary subsystems and the pentenary mixture agree with experimental data at 313.6 K from the present work. Overall, the performance of molecular simulation and COSMO-SAC is very similar. The dependence of the Henry's law constant of pure carbon dioxide and of pure oxygen was studied for both ternary solvent mixtures by molecular simulation and COSMO-SAC. It was found that the agreement with the present experimental data is very good.

It was shown that molecular simulation and COSMO-SAC have a similar performance for the prediction and description of fluid-phase coexistence data, despite the fact that the former carries spatially resolved information on the molecular interactions, whereas the latter does not. Both methods are capable to predict multicomponent VLE with an excellent accuracy, if one state-independent binary parameter is introduced. Beside these satisfactory results, it was found that improvements are necessary, especially when no experimental binary data are available. In predictive mode, deviations up to 50% in terms of the vapor pressure or the Henry's law constant were encountered for some systems.

The presented data and models can be used for the optimization of the reaction conditions for the oxidation of cyclohexane in carbon dioxide expanded liquids. Furthermore, the considered force field models may be used for molecular simulation studies of the behavior of this mixture within nanostructured sieves.^{72–74}

Acknowledgments

The authors gratefully acknowledge financial support by Deutsche Forschungsgemeinschaft, Collaborative Research Centre SFB 706 "Selective Catalytic Oxidations Using Molecular Oxygen", by German Academic Exchange Service (DAAD Doktorandenstipendium Nr. D/11/42734), and from grants NSC100-2811-E-002-067 and NSC 98-2221-E-002-087-MY3 by the National Science Council of Taiwan. The presented research was conducted under the auspices of the Boltzmann-Zuse Society of Computational Molecular Engineering (BZS). Molecular simulations were performed on the national super computer Laki at the High Performance Computing Centre Stuttgart (HLRS) under the grant MMHBF2 and on the HP XC4000 supercomputer at the Steinbuch Centre for Computing (SCC), Karlsruhe, with resources allocated according to the grant MOCOS. The COSMO-SAC calculations were performed on the National Center for High-Performance Computing of Taiwan.

Literature Cited

- Weissermel K, Arpe H-J. *Industrial Organic Chemistry*. Weinheim: VCH Press, 1997.
- Schurz F, Bauchert JM, Merker T, Schleid T, Hasse H, Gläser R. Octahedral molecular sieves of the type K-OMS-2 with different particle sizes and morphologies: impact on the catalytic properties in the aerobic partial oxidation of benzyl alcohol. *Appl Catal A*. 2009;355:42–49.
- Thyessen N, Hou Z, Leitner W. Selective oxidations of alkanes with molecular oxygen and acetaldehyde in compressed (supercritical) carbon dioxide as reaction medium. *Chem Eur J*. 2006;12:3401–3409.
- Seki T, Baiker A. Catalytic oxidations in dense carbon dioxide. *Chem Rev*. 2009;109:2409–2454.
- Merker T, Franke N, Gläser, R, Schleid, T, Hasse, H. Gas solubility in binary liquid mixtures: carbon dioxide in cyclohexane + cyclohexanone. *J Chem Eng Data*. 2011;56:2477–2481.

6. Merker T, Vrabec J, Hasse H. Molecular simulation study on the solubility of carbon dioxide in mixtures of cyclohexane + cyclohexanone. *Fluid Phase Equilib.* 2012;315:77–83.
7. Merker T, Vrabec J, Hasse H. Gas solubility of carbon dioxide and of oxygen in cyclohexanol by experiment and molecular simulation. *J Chem Thermodyn.* 2012;49:114–118.
8. Esmelindro MC, Antunes OAC, Franceschi E, Borges GR, Corazza ML, Oliveira JV, Linhares W, Dariva C. Phase behavior of the reactant and products of cyclohexane oxidation in compressed CO₂. *J Chem Eng Data.* 2008;53:2050–2055.
9. Case F, Chaka A, Friend DG, Frurip D, Golab J, Johnson R, Moore J, Mountain RD, Olson J, Schiller M, Storer J. The first industrial fluid properties simulation challenge. *Fluid Phase Equilib.* 2004;217:1–10.
10. Case F, Chaka A, Friend DG, Frurip D, Golab J, Gordon P, Johnson R, Kolar P, Moore J, Mountain RD, Olson J, Ross R, Schiller M. The second industrial fluid properties simulation challenge. *Fluid Phase Equilib.* 2005;236:1–14.
11. Case FH, Brennan J, Chaka A, Dobbs KD, Friend DG, Frurip D, Gordon PA, Moore J, Mountain RD, Olson J, Ross RB, Schiller M, Shen VK. The third industrial fluid properties simulation challenge. *Fluid Phase Equilib.* 2007;260:153–163.
12. Case FH, Brennan J, Chaka A, Dobbs KD, Friend DG, Gordon PA, Moore JD, Mountain RD, Olson JD, Ross RB, Schiller M, Shen VK, Stahlberg EA. The fourth industrial fluid properties simulation challenge. *Fluid Phase Equilib.* 2008;274:2–9.
13. Case FH, Chaka A, Moore JD, Mountain RD, Olson JD, Ross RB, Schiller M, Shen VK, Stahlberg EA. The fifth industrial fluid properties simulation challenge. *Fluid Phase Equilib.* 2009;285:1–3.
14. Klamt A. Conductor-like screening model for real solvents: a new approach to the quantitative calculation of solvation phenomena. *J Phys Chem.* 1995;99:2224–2235.
15. Wang S, Sandler SI, Cheng CC. Refinement of COSMO-SAC and the Applications. *Ind Eng Chem Res.* 2007;46:7275–7288.
16. Grensemann H, Gmehling J. Performance of a conductor-like screening model for real solvents model in comparison to classical group contribution methods. *Ind Eng Chem Res.* 2005;44:1610–1624.
17. Shimoyama Y, Iwai Y. Development of activity coefficient model based on COSMO method for prediction of solubilities of solid solutes in supercritical carbon dioxide. *J Supercrit Fluids.* 2009;50:210–217.
18. Peng DY, Robinson DB. A new two-constant equation of state. *Ind Chem Eng Fundam.* 1976;15:59–64.
19. Aspen Plus Unit Operation Models, Burlington, MA: Aspen Technology Inc., 2007.
20. Klamt A, Jonas V, Burger T, Lohrenz JCW. Refinement and parametrization of COSMO-RS. *Phys Chem A.* 1998;102:5074–5085.
21. Klamt A. COSMO-RS: From Quantum Chemistry to Fluid Phase Thermodynamics and Drug Design. New York: Elsevier, 2005.
22. Lin ST, Sandler SI. A priori phase equilibrium prediction from a segment contribution solvation model. *Ind Eng Chem Res.* 2002;41:899–913.
23. Hsieh CM, Sandler SI, Lin ST. Improvements of COSMO-SAC for vapor-liquid and liquid-liquid equilibrium predictions. *Fluid Phase Equilib.* 2010;297:90–91.
24. Fredenslund A, Gmehling J, Rasmussen P. Vapor-liquid Equilibria Using UNIFAC. New York: Elsevier Scientific, 1977.
25. DMol3, Material Studio Release 5.5. San Diego, CA: Accelrys Software Inc., 2010.
26. Mullin, E, Oldland R, Liu YA, Wang S, Sandler SI, Chen C-C, Zwolak M, Seavey KC. Sigma-profile database for using COSMO-based thermodynamic methods. *Ind Eng Chem Res.* 2006;45:4389–4415.
27. Mullins E, Liu YA, Ghaderi A, Fast SD. Sigma profile database for predicting solid solubility in pure and mixed solvent mixtures for organic pharmacological compounds with COSMO-based thermodynamic methods. *Ind Eng Chem Res.* 2008;47:1707–1725.
28. Available at: <http://www.design.che.vt.edu/VT-Databases.html>.
29. Franke R, Hannebauer B, Jung S. A case study in the pre-calculation of Henry coefficients. *Chem Eng Technol.* 2010;33:251–257.
30. Franke R, Hannebauer B. On the influence of basis sets and quantum chemical methods on the prediction accuracy of COSMO-RS. *Phys Chem Chem Phys.* 2011;13:21344–21350.
31. Stryjek R, Vera JH. PRSV—an improved Peng-Robinson equation of state for pure compounds and mixtures. *Can J Chem Eng.* 1986;64:323–333.
32. Michelsen ML. A modified Huron-Vidal mixing rule for cubic equations of state. *Fluid Phase Equilib.* 1990;60:213–219.
33. Xia J, Pérez-Salado Kamps A, Maurer G. Solubility of CO₂ in (CH₃OH + H₂O). *J Chem Eng Data.* 2004;49:1756–1759.
34. Rumpf B. *Untersuchungen zur Löslichkeit reagierender Gase in Wasser und salzhaltigen wässrigen Lösungen.* Ph.D Thesis, University of Kaiserslautern, 1992.
35. Rumpf B, Maurer G. Solubilities of hydrogen cyanide and sulfur dioxide in water at temperatures from 293.14 to 413.14 K and pressures up to 2.5 MPa. *Fluid Phase Equilib.* 1992;81:241–260.
36. Rumpf B, Maurer G. An experimental and theoretical investigation on the solubility of carbon dioxide in aqueous solutions of strong electrolytes. *Ber Bunsen-Ges Phys Chem.* 1993;97:85–97.
37. Pérez-Salado Kamps A, Meyer E, Rumpf B, Maurer G. Solubility of CO₂ in aqueous solutions of KCl and in aqueous solutions of K₂CO₃. *J Chem Eng Data.* 2007;52:817–832.
38. Schmidt R, Wagner W. A new form of the equation of state for pure substances and its application to oxygen. *Fluid Phase Equilib.* 1985;19:175–200.
39. Span R, Wagner W. A new equation of state for carbon dioxide covering the fluid region from the triple-point temperature to 1100 K at pressures up to 800 MPa. *J Phys Chem Ref Data.* 1996;25:1509–1596.
40. Stoll J. *Molecular Models for the Prediction of Thermophysical Properties of Pure Fluids and Mixtures.* In: VDI F-B, editor, Reihe 3, 863. Düsseldorf: VDI-Verlag, 2005.
41. Merker T, Engin C, Vrabec J, Hasse H. Molecular model for carbon dioxide optimized to vapor-liquid equilibria. *J Chem Phys.* 2010;132:234512.
42. Merker T, Vrabec J, Hasse H. Engineering molecular models: efficient parameterization and cyclohexanol as case study. *Soft Mater.* 2012;10:3–24.
43. Schnabel T, Vrabec J, Hasse H. Unlike Lennard-Jones parameters for vapor-liquid equilibria. *J Mol Liq.* 2007;135:170–178.
44. Fredenslund A, Sather GA. Gas-liquid equilibrium of the oxygen-carbon dioxide system. *J Chem Eng Data.* 1970;15:17–22.
45. Wilhelm E, Battino R. The solubility of gases in liquids. 5. The solubility of N₂, O₂, CO, and CO₂ in cyclohexane at 283 to 313 K. *J Chem Thermodyn.* 1973;5:117–120.
46. Gallardo MA, Melendo JM, Urieta JS, Gutierrez Losa C. Solubility of non-polar gases in cyclohexanone between 273.15 and 303.15 K at 101.32 kPa partial pressure of gas. *Can J Chem.* 1987;65:2198–2202.
47. Boublik T, Lu BCY. Vapor-liquid equilibria of the cyclohexane-cyclohexanone system at 323.15 and 348.15 K. *J Chem Eng Data.* 1977;22:331–333.
48. Chevalley J. Pressions de vapeur et coefficients d'activité des systèmes phenol-tétrachlorure de carbone et cyclohexanol-cyclohexane. *Bull Soc Chim Fr.* 1961;52:510–515.
49. Gorodetskii IY, Olevskii VM. *Tr Gosudarst Nauch-Issled I Proekt Inst Azot Prom.* 1959;10:99–112.
50. Shing KS, Gubbins KE, Lucas K. Henry constants in nonideal fluid mixtures. Computer simulation and theory. *Mol Phys.* 1988;65:1235–1252.
51. Vrabec J, Hasse H. Grand equilibrium: vapour-liquid equilibria by a new molecular simulation method. *Mol Phys.* 2002;100:3375–3383.
52. Staverman AJ. The entropy of high polymer solutions—generalization of formulae. *Recueil Des Travaux Chimiques Des Pays-Bas-J Royal Netherlands Chem Soc.* 1950;60:163–174.
53. Guggenheim EA. *Mixtures.* Oxford: Oxford University Press, 1952.
54. Hsieh C-M, Lin S-T. First-principles predictions of vapor-liquid equilibria for pure and mixture fluids from the combined use of cubic equations of state and solvation calculations. *Ind Eng Chem Res.* 2009;48:3197–3205.
55. Hsieh C-M, Lin S-T. Prediction of liquid-liquid equilibrium from the Peng-Robinson plus COSMO-SAC equation of state. *Chem Eng Sci.* 2010;65:1955–1963.
56. Lin S-T, Chang J, Wang S, Goddard WA, Sandler SI. Prediction of vapor pressures and enthalpies of vaporization using a COSMO solvation model. *J Phys Chem A.* 2004;108:7429–7439.
57. Hasan O, Stanley SI, Arvind V. *Modeling Vapor-Liquid Equilibria: Cubic Equations of State and Their Mixing Rules.* Cambridge: Cambridge University Press, 1998.
58. Rowley RL, Wilding WV, Oscarson JL, Yang Y, Zundel NA, Daubert TE, Danner RP. DIPPR® Data Compilation of Pure Compound Properties, Design Institute for Physical Properties, AIChE, New York, 2006.
59. Wild JD, Sridhar T, Potter OE. Solubility of nitrogen and oxygen in cyclohexane. *Chem Eng J.* 1978;15:209–214.
60. Naumenko NK. *Investigation on the Solubility of Oxygen in Organic Solvents.* Ph.D Thesis, Leningrad University, 1970.

61. Cauquil G. *J Chim Phys Phys-Chim Biol.* 1926;24:53–55.
62. Chen J-T, Lee M-J. Vapor-liquid equilibria of cyclohexanol with carbon dioxide, ethane, or nitrogen at elevated pressures. *J Chem Eng Data.* 1996;41:339–343.
63. Gironi F, Lavecchia R. A simple method for determining the solubility of gases in liquids: application to CO₂-cycloparaffin systems. *Fluid Phase Equilib.* 1993;87:153–161.
64. Patyi L, Furmer IE, Makranczy J, Sadilenko AS, Stepanova ZG, Berengarten MG. Solubilities of gases in certain organic liquids. *J Appl Chem. (Russ.)* 1978;51:1240–1243.
65. Dymond J. The solubility of a series of gases in cyclohexane and DMSO. *J Phys Chem.* 1967;71:1829–1831.
66. Melendo J, Gallardo M, Urieta J, Gutierrez Losa C. Parametros del potencial intermolecular de la ciclohexanona a partir de medidas de solubilidad de gases. *Acta Cient Compostelana.* 1985;12:269–284.
67. Begley JW, Maget HJR, Williams B. Solubility of carbon dioxide in cyclohexanol, 1,2-dibromoethane, a mixture of 1-chloro-2-bromopropane and 2-chloro-1-bromopropane, and mineral oil. *J Chem Eng Data.* 1965;10:4–8.
68. Shibata SK, Sandler SI. High pressure vapor-liquid equilibria of mixtures of nitrogen, carbon dioxide, and cyclohexane. *J Chem Eng Data.* 1989;34:419–424.
69. Laugier S, Richon D. High-pressure vapor-liquid equilibria of two binary systems: carbon dioxide + cyclohexanol and carbon dioxide + cyclohexanone. *J Chem Eng Data.* 1997;42:155–159.
70. Feng Y, Hu W, Hou Y. Gas-liquid equilibria for carbon dioxide-cyclohexane and carbon dioxide-cyclohexanone systems. *Gaoxiao Huaxue Gongcheng Xuebao.* 1992;6:19–24.
71. Shim H-S, Kim J-S. The prediction of vapor-liquid equilibrium data for cyclohexanol-cyclohexanone system at subatmospheric pressure. *J Korean Ind Eng Chem.* 1999;10:677–681.
72. Schlier J. Carbon dioxide separation with a two-dimensional polymer membrane. *ACS Appl Mater Interfaces.* 2012;7:3745–3752.
73. Brochart L, Vandamme M, Pellenq RJ-M, Fen-Chong T. Adsorption-induced deformation of microporous materials: coal swelling induced by CO₂-CH₄ competitive adsorption. *Langmuir.* 2012;28:2659–2670.
74. Piotr K. Molecular insight into the high selectivity of double-walled carbon nanotubes. *Phys Chem Chem Phys.* 2012;14:2784–2790.
75. Vrabc J, Kettler M, Hasse H. Chemical potential of quadrupolar two-centre Lennard-Jones fluids by gradual insertion. *Chem Phys Lett.* 2002;356:431–436.
76. Widom B. Some topics in the theory of fluids. *J Chem Phys.* 1963;39:2808–2812.
77. Allen MP, Tildesley DJ. *Computer Simulations of Liquids.* Oxford: Clarendon Press, 1987.
78. Anderson HC. Molecular dynamics simulations at constant pressure and/or temperature. *J Chem Phys.* 1980;72:2384–2393.
79. Lustig R. Angle-average for the powers of the distance between two separated vectors. *Mol Phys.* 1988;65:175–179.
80. Flyvbjerg H, Petersen HG. Error estimates on averages of correlated data. *J Chem Phys.* 1989, 91, 461–466.
81. Deublein S, Eckl B, Stoll J, Lishchuk, SV, Guevara-Carrion G, Glass CW, Merker T, Bernreuther M, Hasse H, Vrabc J. ms2: a molecular simulation tool for thermodynamic properties. *Comp Phys Commun.* 2011;182:2350–2367.

Appendix: Simulation Details

In this work, the Grand Equilibrium method⁵¹ was used for VLE simulations. To determine the chemical potential in the liquid, gradual insertion⁷⁵ or Widom's insertion method⁷⁶ was used. For low temperatures near the triple point, gradual

insertion yields results with much lower statistical uncertainties than Widom's method.

Widom's method was applied in conjunction with molecular dynamics simulations in the isothermal-isobaric (*NpT*) ensemble using isokinetic velocity scaling⁷⁷ and Andersen's barostat.⁷⁸ There, the number of molecules was 1372 and the time step was 1 fs. The initial configuration was a face centered cubic lattice, the fluid was equilibrated over 60,000 time steps with the first 10,000 time steps in the canonic (*NVT*) ensemble. The production run went over 400,000 time steps with a piston mass of 10⁹ kg/m⁴. Up to 5000 test molecules were inserted every production time step.

Gradual insertion was applied in conjunction with Monte Carlo simulations in the *NpT* ensemble using 1372 molecules. Starting from a face centered cubic lattice, 15,000 Monte Carlo cycles were performed for equilibration with the first 5000 cycles in the *NVT* ensemble and 100,000 cycles for production. Each cycle contained 1372 displacement moves, 1372 rotation moves, and 1 volume move. Every 50 cycles, 13,720 fluctuating state change moves, 13,720 fluctuating particle translation/rotation moves and 68,600 biased particle translation/rotation moves were performed to determine the chemical potential.

For the corresponding vapor, Monte Carlo simulations in the pseudo- μVT ensemble were conducted. The simulation volume was adjusted to lead to an average number of 864 molecules in the vapor phase. After 10,000 initial *NVT* Monte Carlo cycles, starting from a face centered cubic lattice, 25,000 equilibration cycles in the pseudo- μVT ensemble were performed. The length of the production run was 100,000 cycles. One cycle is defined here to be a number of attempts to displace and rotate molecules equal to the actual number of molecules plus three insertion and three deletion attempts.

The Henry's law constant was determined by calculating the chemical potential with Widom's method or gradual insertion. The technical parameters were the same as those for the liquid runs during VLE calculations. When gradual insertion was used, one solute molecule and 999 solvent molecules were considered to account for infinite dilution.

The cut-off radius was set to at least 15 Å and a center of mass cut-off scheme was employed. LJ long-range interactions beyond the cut-off radius were corrected as proposed by Lustig.⁷⁹ The electrostatic long-range interactions were approximated by a resulting molecular dipole and corrected with the reaction field method.⁷⁷ Statistical uncertainties of the simulated values were estimated by a block averaging method.⁸⁰

All molecular simulation data were obtained with *ms2*.⁸¹

Manuscript received Jun. 12, 2012, revision received Aug. 30, 2012, and final revision received Nov. 30, 2012